



ELSEVIER

Atmospheric Research 67–68 (2003) 607–627

ATMOSPHERIC
RESEARCH

www.elsevier.com/locate/atmos

Satellite observations of convective storm tops in the 1.6, 3.7 and 3.9 μm spectral bands

Martin Setvák^{a,*}, Robert M. Rabin^b,
Charles A. Doswell III^c, Vincenzo Levizzani^d

^a*Czech Hydrometeorological Institute, Satellite Department, Na Šabatce 17, CZ-14306 Praha 4, Czech Republic*

^b*NOAA/National Severe Storms Laboratory, 1313 Halley Circle, Norman, OK 73069, USA*

^c*Cooperative Institute for Mesoscale Meteorological Studies, University of Oklahoma,
Norman, OK 73019-1011, USA*

^d*National Council of Research, Institute of Atmospheric Sciences and Climate, ISAC-CNR,
via Gobetti 101, I-40129 Bologna, Italy*

Accepted 28 March 2003

Abstract

Spatial and temporal characteristics of convective storm tops observed in the 1.6, 3.7 or 3.9 μm and visible satellite spectral bands were examined. National Oceanic and Atmospheric Administration (NOAA)/Advanced Very High Resolution Radiometer (AVHRR) observations over Europe during the 1980s have shown that some storms exhibit a significant increase in the 3.7 μm cloud top reflectivity. Subsequent NOAA/AVHRR observations have shown that similar cloud top phenomena can be found as well for convective storms over the US Great Plains. The launch of the Geostationary Operational Environmental Satellite (GOES)-8, 9 and 10 has enabled the study of the evolution of storm cloud top structures in a similar band (3.9 μm) with high temporal resolution. This imagery shows that the smallest areas of increased 3.9 μm reflectivity (within or above storm tops) appear and fade on the scale of a few minutes, although larger ones can persist for tens of minutes to several hours. Occasionally, cloud top structures resembling plumes have been observed above some of the storms, apparently emanating from cores of these.

Selected cases of convective storms exhibiting an increase in the 3.9 μm reflectivity have been studied with respect to internal storm structure as observed by NEXRAD Doppler radars. This revealed that the spots or areas with increased 3.9 μm reflectivity were typically found above relatively weak radar echo regions, though close to storm cores. However, a few of these “spots” have appeared above a mesocyclone near the time of associated tornado touchdown, suggesting that these spots might be the result of relatively small ice crystals present near the top of strong updrafts. One case of high 3.9 μm reflectivity over an entire storm top has been recorded simultaneously by

* Corresponding author. Fax: +420-24403-2442.

E-mail address: setvak@chmi.cz (M. Setvák).

GOES-8 and GOES-9 on 22–23 May 1996. Some aspects of bidirectional scattering are evident from the differences in 3.9 μm reflectivity observed from these two satellites.

Finally, the appearance of storm tops is compared from observations in the 3.7 or 3.9 μm bands with those in the AVHRR/3 1.6 μm band, which has been recently implemented on NOAA-KLM polar orbiting satellites.

© 2003 Elsevier B.V. All rights reserved.

Keywords: Convective storm tops; Satellites; Spectral bands

1. Introduction

Satellite imagery in the visible and 10–12.5 μm spectral regions have provided useful observations of thunderstorm anvils, overshooting tops and associated cloud top temperature patterns, such as the enhanced “V” and warm wake since the 1970s (e.g., Adler and Mack, 1986). Additional cloud top information has been revealed with the advent of imagery from 3.5 to 4.0 μm wavelengths. For example, the Geostationary Operational Environmental Satellite (GOES) 8, 9, 10 channel 2 (3.78–4.03 μm) and the National Oceanic and Atmospheric Administration (NOAA)/Advanced Very High Resolution Radiometer (AVHRR) channel 3B (3.55–3.93 μm), both cover a spectral band that includes emitted and reflected solar radiation during the daytime, represent a unique observational tool for studies of the microphysics of convective storm cloud tops. Given the very low temperatures of anvil tops, the emitted component in these channels is relatively small. Hence, the reflected component plays the major role in appearance of convective storms in these channels during daytime hours (Setvák, 1989).

Daytime observations over Europe from NOAA/AVHRR data have shown that some convective storms exhibit a significant increase in the 3.7 μm cloud top reflectivity and that the observed features fall into two broad classes (Setvák and Doswell, 1991):

- (1) Either small spot-like areas of increased 3.7 μm reflectivity, typically located close to overshooting tops as determined from visible (VIS) imagery, or more widespread irregular areas (of increased 3.7 μm reflectivity) with fuzzy or blurred edges. These features range in size from that of a single AVHRR pixel ($1 \times 1 \text{ km}^2$) to the extent of the entire anvil top.
- (2) A plume-like shape (hereafter referenced as “plume”), emanating from almost a pixel-size source, typically located downwind from the coldest tops (Levizzani and Setvák, 1996). This form has been observed much less frequently than the other class.

Melani et al. (2003a,b) have recently successfully simulated the reflectance at 3.7 μm and the brightness temperature at 11 μm of a plume over a large storm using several ice crystal habits and dimensions. Their findings suggest that very small ice crystals (4–6 μm) are responsible for the enhanced reflectivity values of plumes and that the effect disappears with increasing crystal size.

Wang (2001) has used a 3D quasi-compressible, time-dependent, non-hydrostatic cloud model with explicit microphysics on the 02 August 1981 Cooperative Convective Precipitation Experiment (CCOPE) supercell storm to simulate plume formation. The model was run at very fine vertical resolution (0.2 km) and the sounding data, which originally did not contain moisture information above 300 hPa, were integrated with an average water vapor profile over midlatitudes (40–60°N) from the Halogen Occultation Experiment (HALOE) satellite. No plume formation is detected before 20 min into the simulation and at 24 min, a gravity wave motion is visible. A surge of high humidity appears above the second wave crest, propagating upward and westward (upstream relative to the upper level wind direction) into the stratosphere. The water vapor structure then detaches from the anvil and develops into a plume-like feature that largely resembles that described by Fujita (1982).

Research carried out between 1994 and 1997 (supported by the US/Czechoslovak Science and Technology Program, Project #94067) extended the previous European observations of features with enhanced 3.7 μm reflectivity to the US Great Plains. This research made use of geostationary satellite and Doppler radar observations in addition to AVHRR data used in the previous studies. The introduction of the GOES 8, 9, 10 satellites since 1994 (Menzel and Purdom, 1994) enables determination of the *evolution* of the cloud top phenomena, with temporal sampling rates from 15 min down to 30 s (according to scanning mode of the satellite). Doppler radar in the US (Doviak and Zrníć, 1984) can be used to help link the observed cloud top features to internal storm structure, which is not available from satellite observations alone. A goal of this paper is to provide some examples of plume and area of high reflectivity durations, and their location with respect to internal storm structure, within the limitations of Doppler radar to depict that structure, of course.

Additionally, the 1.6 μm spectral band is expected to have similar capabilities of cloud top characteristics determination as the 3.7 or 3.9 μm bands and the 2.1 μm band (e.g., King et al., 1992; Nakajima and King, 1992; Nakajima and Nakajima, 1995). The 1.6 μm band is presently available on the AVHRR/3 of NOAA-16 and 17, the Moderate Resolution Imaging Spectroradiometer (MODIS) of the National Aeronautics and Space Administration (NASA) Earth Observing System (EOS) TERRA and AQUA satellites, and the Spinning Enhanced Visible and InfraRed Imager (SEVIRI) of Meteosat Second Generation (MSG), (Schmetz et al., 2002). The major advantage of the 1.6 μm band is that the emitted component is negligible (as compared to the solar reflected component) and therefore the detected radiance in this band can be treated as of reflected origin. This makes its interpretation and utilization more straightforward as compared to the 3.7 or 3.9 μm bands. However, Rosenfeld et al. (2002) have recently shown that care must be used while inferring cloud top properties using the 1.6 and 3.7 or 3.9 μm bands, since they measure radiation from different depths in the cloud and are subject to “surface contamination” effects in different ways. This paper documents some of the first comparisons of plumes and high reflectance features observed in the 3.7 or 3.9 μm bands with those in the 1.6 μm band (NOAA-16 AVHRR/3 channel 3A).

Data sources and processing procedures are presented in Section 2. Observations from 3.7 or 3.9 to 1.6 μm bands are presented in Sections 3 and 4, respectively. A summary and conclusion are given in Section 5.

2. Data sources and processing

2.1. NOAA/AVHRR

The NOAA/AVHRR data for the US region have been obtained from the NOAA National Environmental Satellite, Data, and Information Service (NESDIS) Satellite Active Archive (SAA) in NOAA/SAA level-1B format (Goodrum et al., 2000), while data for Europe have been obtained from an archive of the Czech Hydrometeorological Institute (CHMI) in raw High Resolution Picture Transmission (HRPT) format. The AVHRR data sets were processed (calibrated, georeferenced and re-mapped for comparison with GOES images) by software written at CHMI for MS-DOS/Windows platforms and by a commercial software package (ENVI, Research Systems). Daytime data from the AVHRR channel 3B have been converted into 3.7 μm reflectivity by an algorithm developed at CHMI (Setvák and Doswell, 1991). This uses the brightness temperature in the 11 μm band to estimate and remove the thermal emission from the observed radiance at 3.7 μm . The algorithm computes the reflectivity by normalizing the reflected solar radiation by the incident solar radiation.

2.2. GOES-8, 9, 10

Most of the GOES-8, 9, 10 imagery was obtained from the NOAA/NESDIS archive. Data were also supplied from the NESDIS Regional and Mesoscale Meteorological Branch (RAMM) and from the NCAR Cooperative Program for Operational Meteorology, Education, and Training (COMET). Data were processed using the University of Wisconsin Man Computer Interactive Data System (McIDAS).

Daytime reflectivity at 3.9 μm (GOES-8, 9, 10 channel 2) was computed from measured radiance at 3.9 μm and 11 μm (channel 4) following the same method as the one used for computation of the AVHRR 3.7 μm reflectivity (Setvák and Doswell, 1991). Since this method assumes opaque cloud, gaps or optically thin parts of anvil (e.g., its edges) will appear as false “higher 3.9 μm reflectivity” spots or areas. To exclude these from real higher 3.9 μm reflectivity features, GOES VIS (channel 1) data have been used for verification of optical thickness of the clouds.

2.3. Other data

Radar data (WSR-88D) were obtained from the National Climatic Data Center (NCDC) archive for individual radar sites that recorded data in level-II format. Reflectivity and radial velocity data were displayed using the Radar and Algorithm Display System (RADS) developed at the National Severe Storms Laboratory (NSSL). Supplementary surface and rawinsonde observations obtained during the 1995 Verification of the Origins of Rotation in Tornadoes Experiment (VORTEX) in the southern US Plains (Rasmussen et al., 1994) augmented routine meteorological data during this period. Surface observations of hail, high winds, and tornadoes were obtained from the log of severe weather maintained by the NOAA Storm Prediction Center.

3. Observations in the 3.7 and 3.9 μm spectral bands

3.1. NOAA/AVHRR observations and comparison of the AVHRR and GOES-8 measurements

Examination of 30 AVHRR data sets from 1994 to 1995 (NOAA satellite passes with “significant” convection being present) has indicated that the 3.7 μm features (both—“spots” and “plumes”) observed for European storms (Setvák, 1989) can be found also over some of the US Great Plains convective storms. Although the number of investigated cases is much smaller compared to the European observations, these observations indicate a higher *frequency* of spots and plumes than in Europe. No statistical analyses and comparison have been performed given the relatively low total number of the processed US data sets. The majority of plumes are detectable in the AVHRR channels 1 and 2 only, showing no detectable increase of the 3.7 μm reflectivity. However, this may result from the fact that most of these plumes were found on early evening NOAA 12 images, when the low elevation of the sun does not provide enough 3.7 μm radiance to illuminate the scene sufficiently. Despite these ambiguities (resulting very likely from different equator crossing times of satellites used, and therefore different illumination conditions), in general these observations indicate that storm cloud tops have a similar appearance in the AVHRR 3.7 μm channel over both continents.

The most pronounced plume of increased 3.7 μm reflectivity found in the US AVHRR data sets of 1994–1995 is shown on NOAA 11 images from 26 April 1994, at 2250 UTC (Fig. 1). The plume appears to emanate from an older cell in the middle of the image, while upper-level winds carry the particles of the plume from its source to the northeast. As can be seen from the AVHRR channel 2 image (top), the plume appears to be separated vertically from the rest of the anvil. In the 3.7 μm reflectivity image (bottom), the plume appears darker than surrounding clouds (greater thermal radiance) as it is associated with enhanced reflectivity. The plume extends well beyond the edge of storm’s anvil, reaching peak 3.7 μm reflectivity values of around 0.05 to 0.07 (reflectivity ranges from 0 for nonreflective surfaces to 1 for total reflection, whereas the anvil’s mean “background” is around 0.03–0.04. The highest 3.7 μm reflectivity within it reaches 0.106. Notice the almost “point-like” source of this plume close to one of the two small “spots” of high 3.7 μm reflectivity. Since the GOES 3.9 μm band was introduced a year after the occurrence of this storm, development of this plume can be traced only from VIS GOES-7 imagery. The plume appeared first at 2200 UTC and persisted until sunset. (Since plumes are only detected from reflected solar energy in the VIS and 3.7 or 3.9 μm bands, it is not possible to follow their evolution after sunset.)

3.2. Spots in the 3.9 μm GOES-8 channel 2 above convective storms

Seven GOES-8 data sequences, showing deep convective storm developments, have been examined for the presence of spots or plumes of increased 3.9 μm reflectivity above storm tops. Supplementary ground observations were available for a few of these storms, which developed on days of VORTEX operations. Many of the storms did produce spots of varying size, persistence, and magnitude. Lifetimes of these spots

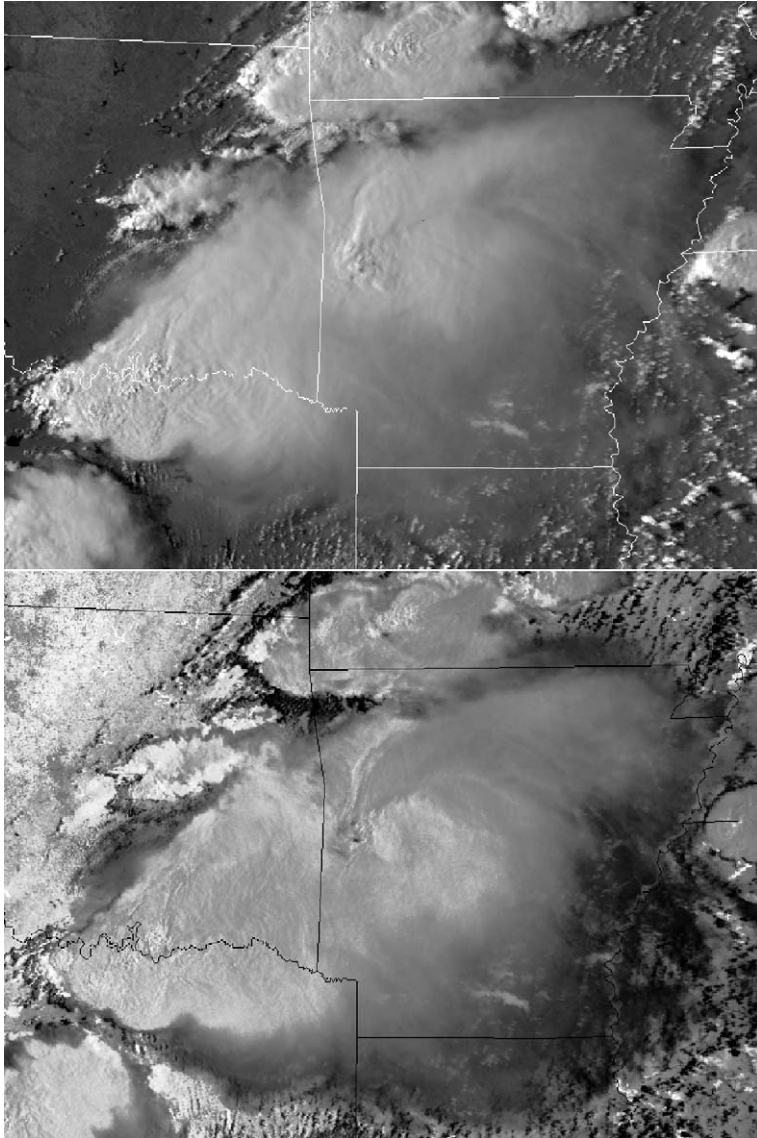


Fig. 1. Convective storms over southeast Oklahoma, west Arkansas and north Texas on 26 April 1994, 2250 UTC, from NOAA 11. Top image: AVHRR channel 2. Bottom image: $3.7 \mu\text{m}$ reflectivity (brightness inversely proportional to reflectivity).

ranged from few minutes (as determined from 1 min data scans) to about 2 h. The width of these varied from that of one single GOES-8 channel 2 pixel (4 km) to about 20–30 km across. Highest recorded $3.9 \mu\text{m}$ reflectivity was about 0.20, while the typical “background” value of the anvils was about 0.02–0.04. The brightness

temperatures of these clouds were below 220 K, which implies an all-ice cloud top (Detwiler et al., 1992). No direct link between the 3.9 μm reflectivity maxima and brightness temperature minima was found, which confirms that overshooting tops can be excluded as preferred areas where the spots of increased 3.9 μm reflectivity occur. Based on these observations, no direct link between hail and increased 3.7 or 3.9 μm reflectivity was found. It had been speculated, from earlier European observations (Setvák, 1989) that such a link might exist. Some of the storms that are known to have produced significant hail on VORTEX days have shown no detectable increase of 3.7 or 3.9 μm reflectivity.

Given the observation that spots of increased 3.9 μm reflectivity do not develop at any specific location with respect to the brightness temperature field and, therefore, are not linked exclusively to overshooting tops. An attempt was made to determine their possible sources using NEXRAD radar reflectivity and radial velocity data. Though only four data sets (07 May 1995, 23 May 1995, 02 June 1995 and 08 June 1995) have been examined in detail, it soon became evident that the characteristics of increased 3.9 μm reflectivity spots are more varied than previously suspected.

Most of the smaller scale spots (1–2 pixels in GOES-8 3.9 μm channel imagery) appear above areas with relatively weak radar reflectivity, lasting from a few minutes up to almost 1 h. In cases when spots appear above storms organized in lines, they typically developed on the northwestward side of a ridge of overshooting tops and later drifted westward (storm-relative) into the “stratiform” part of anvil. Nevertheless, even such spots may have a pronounced “core” from which the ice particles causing increased reflectivity seem to spread out into the surrounding area. The mechanism generating these spots remains unknown.

Another rare category of spots appears (though based on a very small number of found cases) to be linked to mesocyclones and cores of high reflectivity or bounded weak echo regions (BWER) aloft. Their behavior and co-location with a nearby mesocyclone seems to vary significantly. For example, on 07 May 1995 a spot of high 3.9 μm reflectivity (between 0.078 and 0.087, compared to “background” values of about 0.035 to 0.040) appeared above a mesocyclone at 2145 UTC, which also was the reported touchdown time of an associated tornado. The VIS and 3.9 μm images from GOES-8 are shown in Fig. 2a for this time. Locations of the high reflectivity spot and mesocyclone (at 2.5 km AGL; parallax correction was considered in comparing locations between radar and satellite images) with time are given in Fig. 2b. Since the previous 3.9 μm image from 2130 UTC shows no trace of the spot, an uncertainty of up to 15 min remains for the time of the spot’s first appearance. After its formation, the spot immediately began to drift away from its “parent” cell as determined by radar observations. The spot persisted in the anvil for about the next 2 h, disappearing after 2330 UTC.

A second case (not shown here) with a spot above a mesocyclone occurred on 02 June 1995. The spot first appeared at about 2330 UTC (the mesocyclone was first detected at 2246 UTC). The size and reflectivity of the spot was the same at 2345 UTC, and then increased in reflectivity and size by 0015 UTC, attaining a diameter of about 15 km. The spot(s) appears to have been in close proximity to the mesocyclone during this period. However, no GOES-8 image is available to confirm extent and movement of the spot between 2345 and 0015 UTC. A tornado touchdown was reported at 2300 UTC, followed by three more between

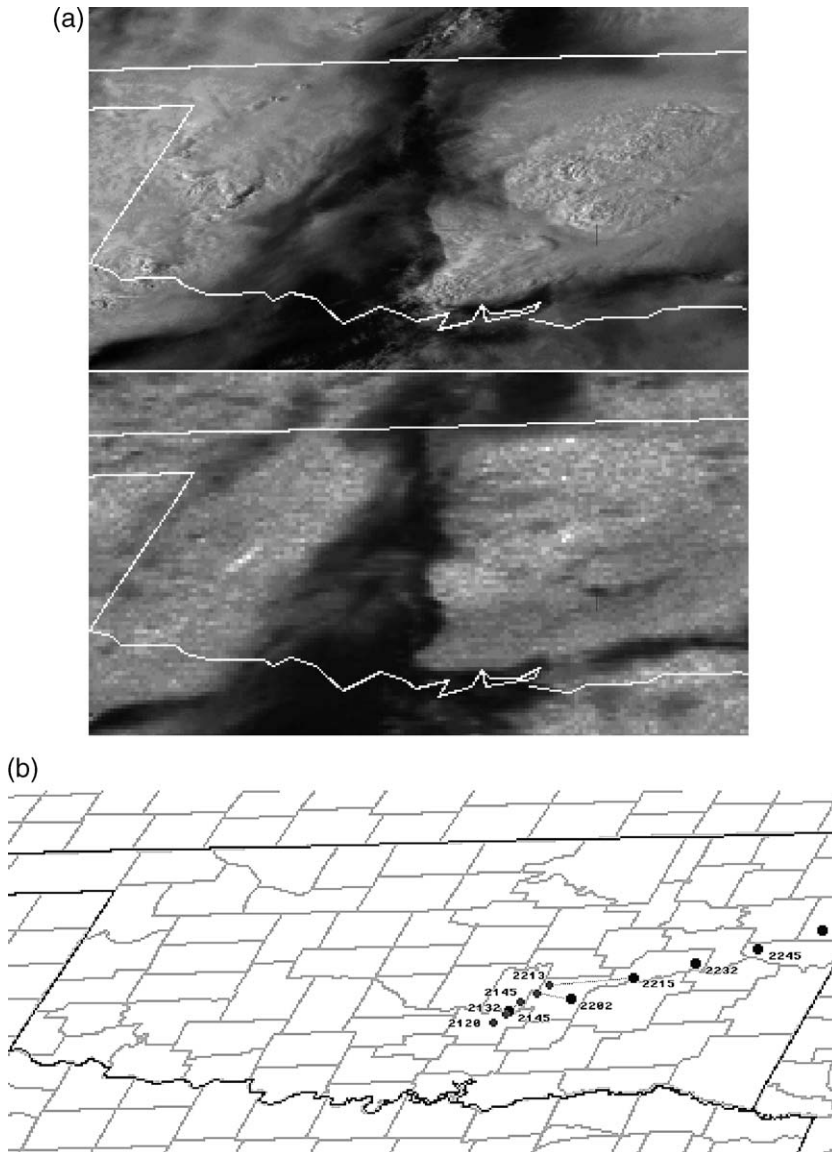


Fig. 2. Tornadoic storm over Oklahoma from 07 May 1995 as seen by GOES-8 at 2145 UTC: (a) channel 1 image (VIS band, top image) and channel 2 image (3.9 μm band, bottom image). Top of the short bar indicates the location of the center of the spot of increased 3.9 μm reflectivity, as seen in the channel 2 image. (b) Positions of the GOES-8 3.9 μm band (channel 2) spot of increased reflectivity at 15-min intervals (larger dots) and location of the associated mesocyclone at approximately 2.5 km level between 2120 and 2213 UTC (smaller dots).

2343 and 0000 UTC (Storm Data, 1995). There was no trace of the spot on the next image taken at 0045 UTC, and the mesocyclone disappeared around 0030 UTC.

3.3. Long-lived plumes of 22–23 May 1996

Deep convective storms with distinct plume-like structures above the anvil tops and overall high 3.9 μm cloud top reflectivity developed over northeastern Colorado and southwestern Nebraska on 22–23 May 1996 (Fig. 3). The first of these storms, which later developed into a major severe weather event within the area, formed at about 1940 UTC (according to NEXRAD observations). A persistent mesocyclone was observed from 2030 until at least 0055 (which was the time of NOAA 12 passage over the area, shortly before sunset). Radar echo heights were at least 14 to 16.5 km for most of the life of the mesocyclone; however, the absolute heights cannot be determined adequately given the radar sampling in elevation (e.g., Maddox et al., 1999). The brightness temperature, from the GOES-8 11- μm channel, decreased almost continuously from the onset of the storms (1940 UTC) to 2330–0100 UTC, when a minimum was reached. A similar trend can be found for the difference between the minimum cloud top temperature and the local maximum, which can be found downstream, within the embedded warm spot (Adler and Mack, 1986). This suggests that the storm was in a mature stage when observed around sunset.

The GOES-8 and GOES-9 VIS imagery (Fig. 3a), and the NOAA 12 AVHRR channel 2 image (Fig. 3b), clearly show a plume, that appears to be above the anvil top (on the basis of shadows observed in the visible imagery). It started to develop around 2145 UTC and persisted until sunset, though variations in the morphology of the plume can be observed during this period.

The height of the plume was determined, from the solar elevation and viewing geometry, to be about 1.2 km above the anvil cloud top from its shadow width in the NOAA 12 AVHRR channel 2 image at 0055 UTC (about 15 km downwind from its apparent source). The plume could not be seen in enhanced thermal IR imagery (AVHRR channel 4). However, it appeared to emanate from near the warm spot, which is typical of such plumes (Levizzani and Setvák, 1996).

Imagery from GOES-8 and GOES-9 channel 2 (3.9 μm , Fig. 3c) at 2045 UTC documents a significant increase of the 3.9 μm reflectivity of one of the storms (the one over south part of Wyoming and Nebraska border). The area of high reflectivity (dark shade) encompassing nearly the width of the entire anvil can be followed until sunset. It was being advected away to the northeast at a speed of $\sim 38 \text{ m s}^{-1}$. A distinct maximum in reflectivity was observed near the leading edge of this feature through the period of observation. Also, the overall 3.9 μm cloud top reflectivity of the entire anvil top was significantly higher than that of the other storms in the area. The significance of the simultaneous onset of the high 3.9 μm cloud top reflectivity and a mesocyclone at 2030–2045 UTC remains uncertain.

A second storm showing similar characteristics developed to the southeast of that described above at about 2200 UTC, though much smaller in horizontal size. The downstream anvil exhibited a high 3.9 μm cloud top reflectivity from the time of its onset, well before persistent mesocyclone activity was observed (from 2320 UTC). The

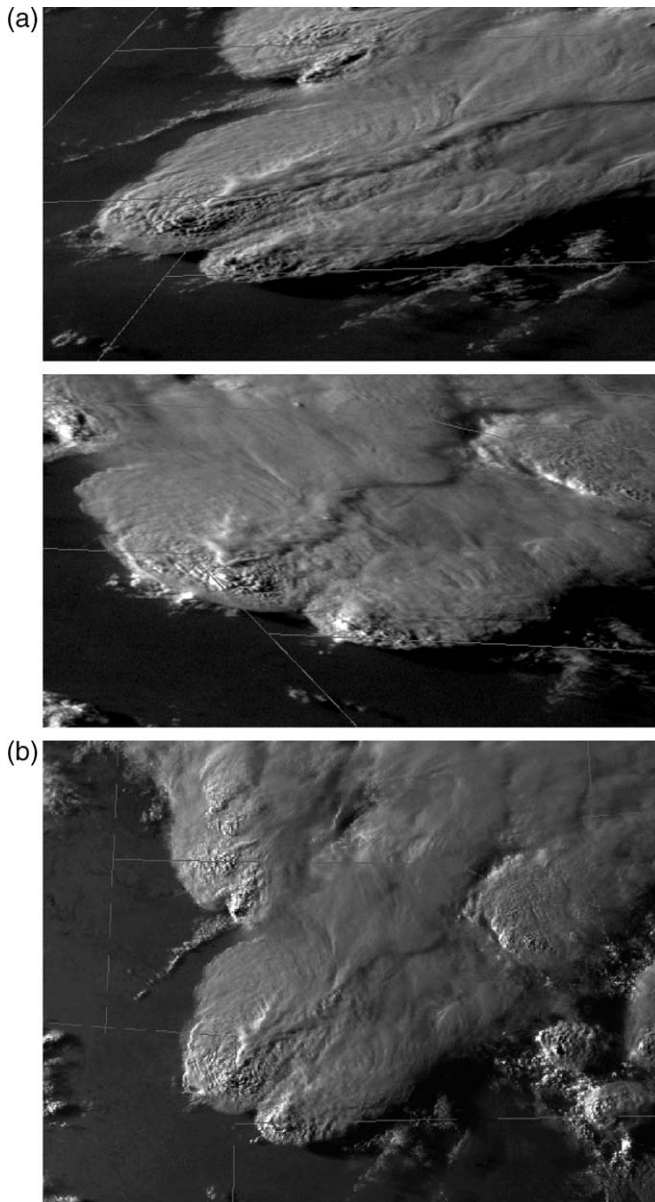


Fig. 3. Tornadoic storms over northeast Colorado and southwest Nebraska on 22–23 May 1996: (a) GOES-8 (top) and GOES-9 (bottom) VIS images at 23 May 1996, 0045 UTC. (b) NOAA 12 (AVHRR channel 2), 23 May 1996, 0055 UTC. (c) Mosaic of GOES-8 (left) and GOES-9 (right) 3.9 μm band images (channel 2, enhanced), showing the evolution of storm's top on 22 May 1996 at 2045, 2130, 2215 and 2300 UTC. (d) Plot of the GOES-8 (upper panel), GOES-9 (lower panel) 3.9 μm reflectivity changes of cloud tops of convective storms over northeastern Colorado and southwest Nebraska on 22 May 1996 (late afternoon sunset). Symbols in the graph represent the evolution of the 3.9 μm reflectivity of: the highest reflectivity area (HRA) within the plume, major storm top (MST) that produced the plume, and cloud top of the low reflectivity storm (LRS) to the northwest of the major storm.

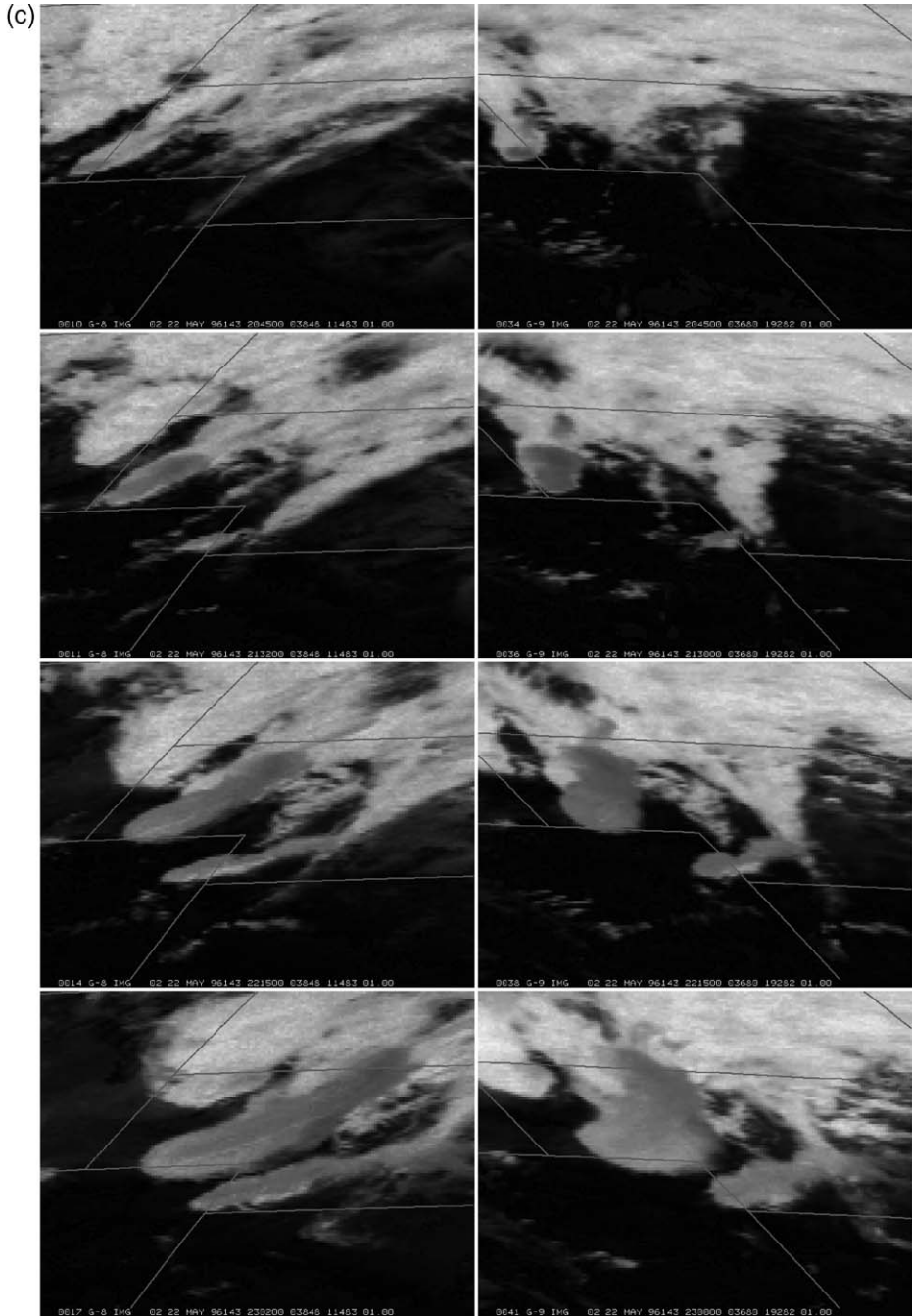


Fig. 3 (continued).

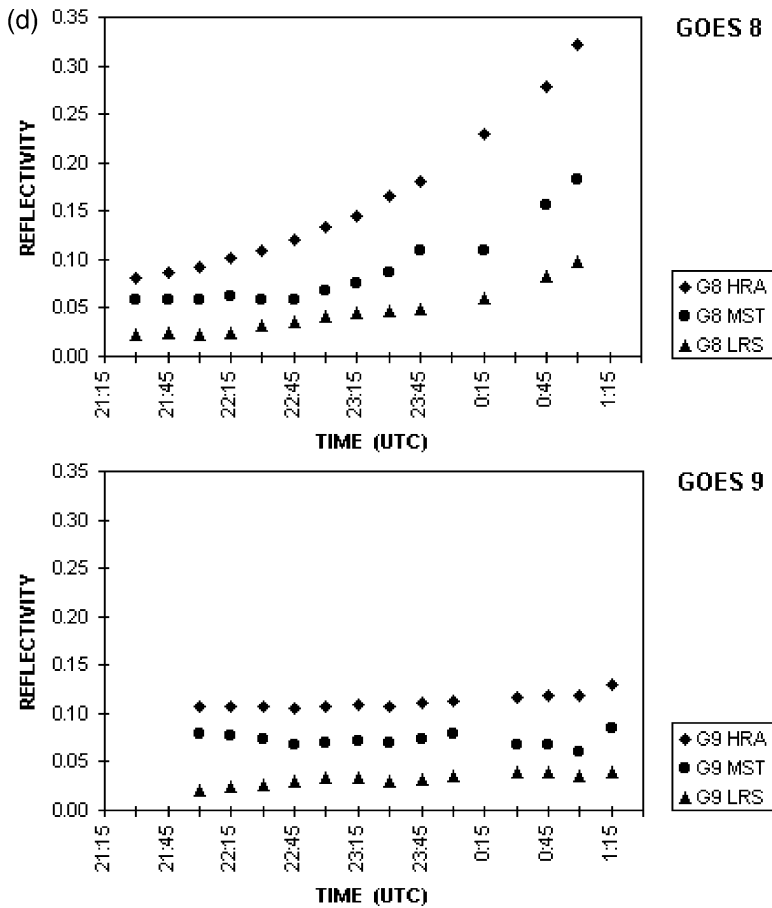


Fig. 3 (continued).

storm also produced a plume evident in VIS imagery, though not as prominent as in the case of the larger storm to the northwest. Other, neighboring storms exhibited only low 3.9 μm cloud top reflectivity and produced no plume at any time during their lifecycles.

As can be seen from Fig. 3d, the 3.9 μm reflectivity values obtained from GOES-8 increase with time while the values from GOES-9 remain relatively constant. The 3.9

Table 1
Azimuthal coordinates of GOES-8 and GOES-9, relative to storm location at 42N/100W

	Elevation	Azimuth
GOES-8 (75W)	35.29°	145.13°
GOES-9 (135W)	30.02°	226.30°

Table 2
Azimuthal coordinates of the sun, relative to storm location at 42N/100W

Time (UTC)	Elevation [degree, $\pm 0.1^\circ$]	Azimuth [degree, $\pm 0.1^\circ$]
2130	47.8	253.1
2200	42.4	259.5
2230	36.9	265.1
2300	31.3	270.3
2330	25.4	275.2
2400	20.3	279.9
0030	14.9	284.5
0100	9.6	289.2
0130	4.5	294.0

μm reflectivity becomes noticeably higher for all selected areas after 2300 (about 3 h before sunset) for GOES-8 as compared to GOES-9 because of more favorable forward scattering angles when observing from the GOES-8 location (Tables 1 and 2). The $3.7 \mu\text{m}$ reflectivity values for NOAA 12 (at 0055 UTC), for which the storms were almost directly at nadir, are 0.08 for the peak within the plume, 0.07 in the background anvil, and 0.03 in the storm to the northwest. These are in the same order as the reflectivities given in Fig. 3d.

Fig. 3d clearly illustrates that 3.7 and $3.9 \mu\text{m}$ reflectivity values of storm tops (ice clouds) are highly sensitive to scattering geometry or, in other words, that cloud tops of convective storms are far from being a Lambertian surface. Thus, the 3.7 and $3.9 \mu\text{m}$ reflectivity values are not only related to cloud top properties (microphysical composition), as has been demonstrated in Melani et al. (2003b), but also to scattering geometry. This may be crucial for those algorithms that utilize either the 3.7 or $3.9 \mu\text{m}$ reflectivity, or the 11 – $3.7 \mu\text{m}$ bands brightness temperature difference as a parameter for automated cloud classification or detection.

4. Observations of storm tops in the $1.6 \mu\text{m}$ spectral band

The recent launch of several satellites (e.g., NOAA-16 and 17, TERRA, AQUA) has enabled observations of storm tops using the $1.6 \mu\text{m}$ band. As previously mentioned, the solar radiance should be scattered (reflected) in this band similarly to the 3.7 and $3.9 \mu\text{m}$ bands. Possible differences in the appearance of storm tops in the $1.6 \mu\text{m}$ versus the 3.7 and $3.9 \mu\text{m}$ bands could result from the fact that very small ice particles are more sensitive to radiation scattered at $1.6 \mu\text{m}$ and, therefore, the scattering conditions are somewhat different. There is about a factor of two in size between the effective radii of the particles sensitive to radiation in the two channels. A complicating factor is that the radiance measured in the $1.6 \mu\text{m}$ band is responsive also to the contributions coming from deeper in the cloud (Rosenfeld et al., 2002).

Fig. 4 shows storms (over eastern Greece and western Turkey) that exhibit large variations of the storm tops reflectivity in the $1.6 \mu\text{m}$ band. Fig. 4a (slightly contrast-enhanced AVHRR channel 2 image) shows several storms in the area. The following discussion focuses on the storms annotated “A” and “B”. Fig. 4b shows the AVHRR

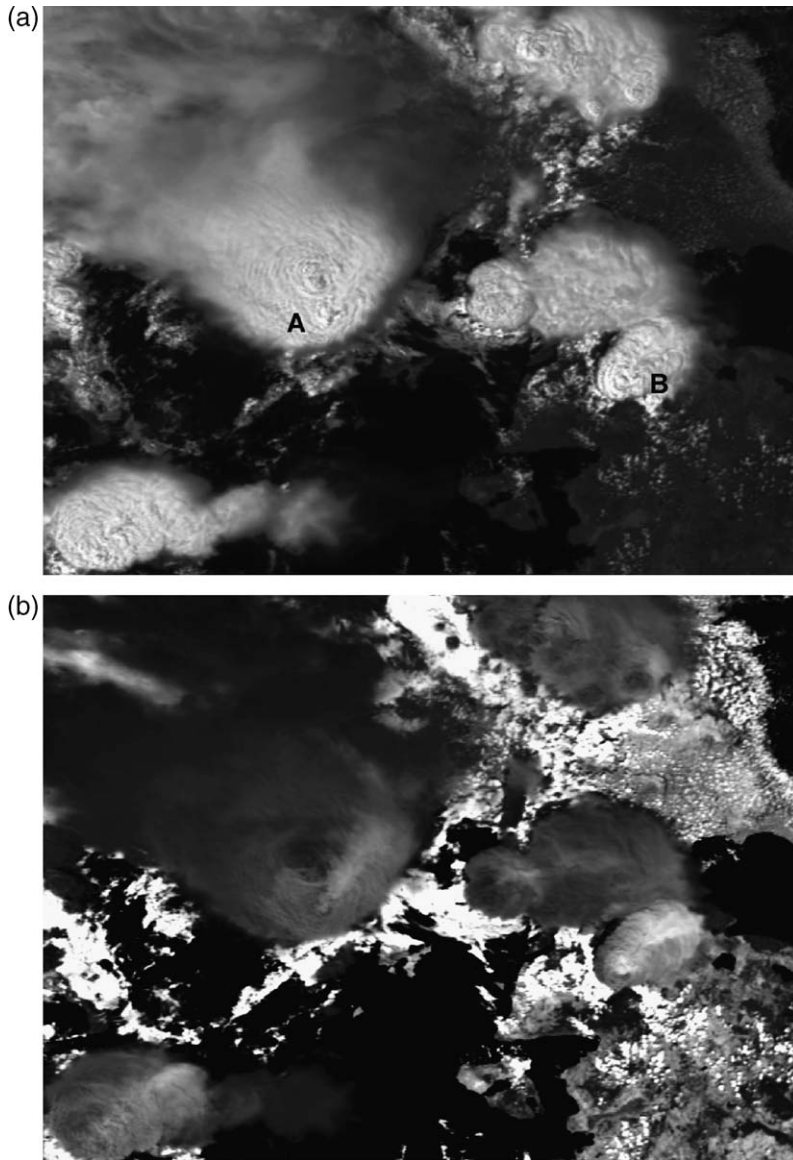


Fig. 4. Storms over southeast Balkan on the 27 July 2002 as seen by NOAA-16 at 1155 UTC: (a) AVHRR/3 channel 2 image (slightly enhanced). (b) AVHRR/3 channel 3A image (1.6 μm band), stronger enhancement. Brightness is proportional to 1.6 μm reflectivity. Low clouds with highest 1.6 μm reflectivity are shown in white, sea level with low reflectivity appears darkest.

channel 3A (1.6 μm band) for the same region as Fig. 4a. As can be seen in this enhanced image (Fig. 4b), the storm tops show variations of the 1.6 μm reflectivity similar to those found in the 3.7 μm imagery. This case also documents the presence of plumes in the 1.6

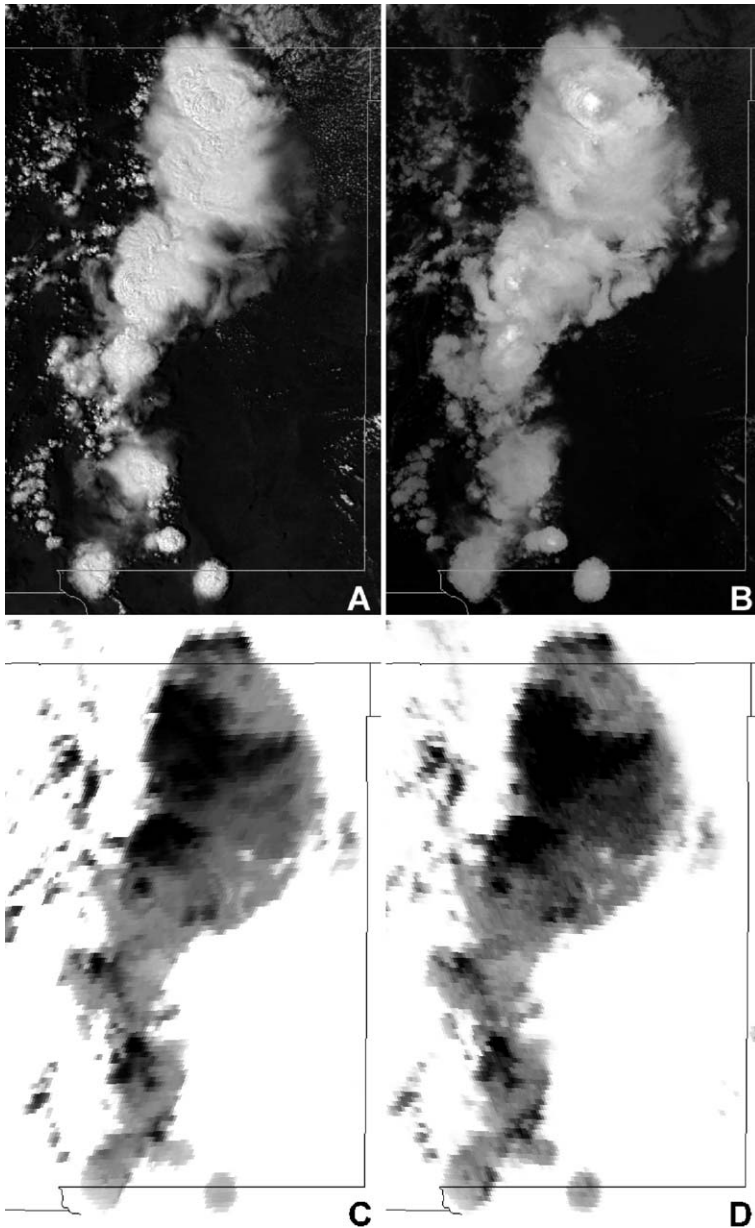


Fig. 5. Storms over eastern part of New Mexico from 11 May 2001 2030 UTC, as seen by NOAA-16 (A, B, E), GOES-10 (C) and GOES-8 (D): (A) NOAA-16, AVHRR channel 2 image. (B) NOAA-16, AVHRR channel 4 image. (C) GOES-10, 3.9 μm band (channel 2). Brightness is inversely proportional to radiance (emitted plus reflected). (D) GOES-8, 3.9 μm band (channel 2). Enhancement as in (C). (E) NOAA-16, 1.6 μm band (AVHRR channel 3A). Brightness is proportional to radiance (reflected).

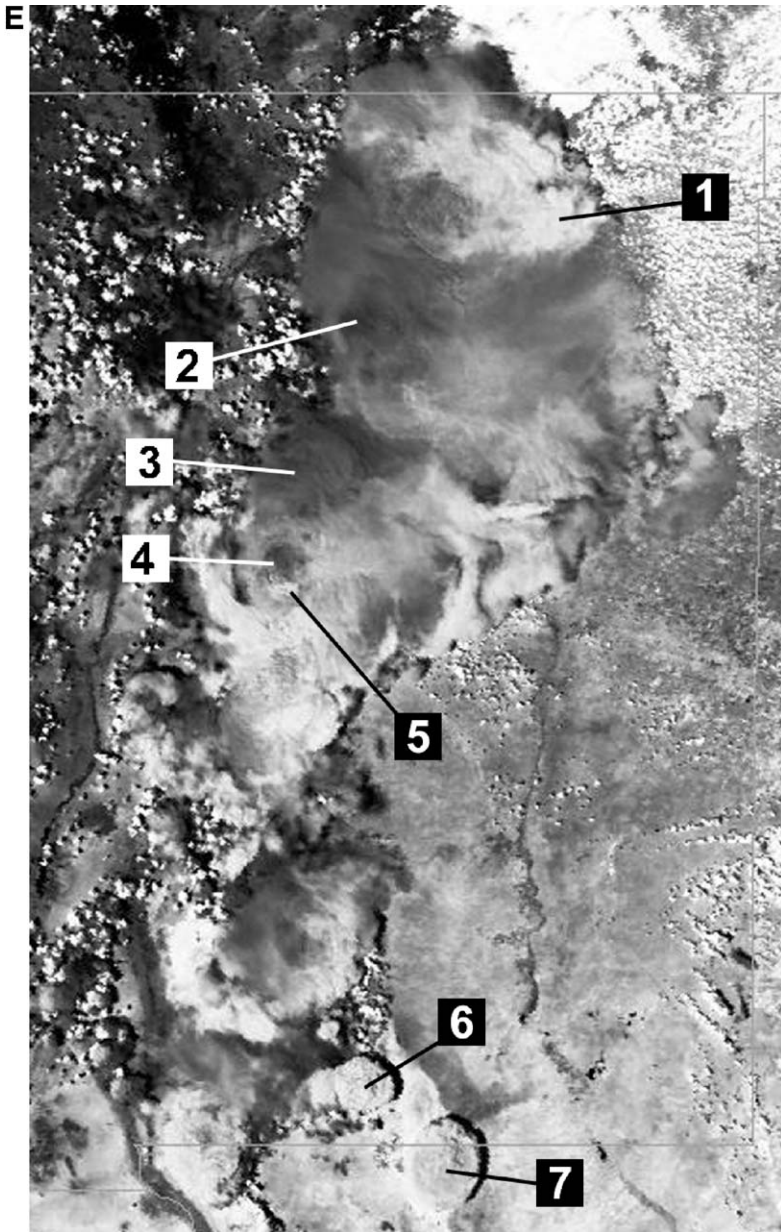


Fig. 5 (continued).

μm imagery (for example above storm “A”). From the AVHRR channel 4 data (not shown), the plume appears to be slightly warmer than the underlying anvil top, at least close to its source.

The plume associated with storm “B” (Fig. 4b) appears to be split or bifurcated, which is rather an uncommon plume characteristic. Though this plume can be resolved in the 1.6 μm bands, there are differences in the exact position and shape of the high 1.6 μm reflectivity area as compared to the position of the plume in the AVHRR channels 2 and 4 images.

Another case is presented in Fig. 5, which shows storms over eastern New Mexico on 11 May 2001 at 2030 UTC. This case provides an opportunity to compare storm tops observed nearly simultaneously in the NOAA-16 1.6 μm band with the GOES-8 and GOES-10 3.9 μm bands. The NOAA and GOES images in Fig. 5 have been remapped to a common map projection with uniform spacing in latitude and longitude (Plate Carree projection). The first two images (Fig. 5A,B) illustrate how these storms appear in the more familiar spectral bands, namely, the NOAA-16 AVHRR channel 2 (Fig. 5A) and the NOAA-16 AVHRR channel 4 (Fig. 5B). The next two images (Fig. 5C,D) document the appearance of these storms in the GOES-10 and GOES-8 3.9 μm band (channel 2), respectively. Unlike the other 3.9 μm band images shown in this paper, the images are enhanced to facilitate comparison with the NOAA-16 1.6 μm image in Fig. 5E. All three images (Fig. 5C–E) depict highly reflective storm tops as almost white or light gray, while dark cloud tops correspond to low reflectivities. Quantitative values of the reflectivities for several selected locations (as indicated in Fig. 5E), together with location’s brightness temperature as derived from the NOAA-16 channel 4 are given in Table 3.

As can be seen by comparison of Fig. 5C–E, all these images show roughly the same general features of storm cloud tops. It should be noted that these images were enhanced to show approximately the same contrast in brightness. The actual values of reflectivities differ quite substantially. One of the reasons for this is the “bidirectional scattering effect” (Section 3). The differences also might result from sensitivity to particle size as the ratio of particle size to wavelength varies between bands. An approach to evaluate this sensitivity is to perform similar comparisons using a single instrument, providing data from both bands with the same viewing angle. This should be possible by using MODIS, or data from the MSG when it becomes operational. The MSG satellite will provide operational data from both these bands (1.6 and 3.9 μm) at 15-min intervals, thus enabling some

Table 3
Reflectivity values (1.6 and 3.9 μm) and 11 μm brightness temperature for different parts of storms shown in Fig. 5E

Location in Fig. 5E	Latitude (North)	Longitude (West)	GOES-10 3.9 μm reflectivity [± 0.002]	GOES-8 3.9 μm reflectivity [± 0.002]	NOAA-16 1.6 μm reflectivity [± 0.001]	NOAA-16 AVHRR channel 4 brightness temperature [K, ± 0.2 K]
1	36.37	104.16	0.093	0.077	0.416	206.1
2	35.91	105.32	0.027	0.023	0.229	210.3
3	35.23	105.75	0.040	0.033	0.238	208.9
4	34.77	105.77	0.041	0.034	0.265	204.2
5	34.65	105.76	0.087	0.064	0.421	211.6
6	32.26	105.32	0.117	0.073	0.429	206.4
7	31.88	104.83	0.104	0.075	0.391	213.5

evolution studies of the reflectivity changes. Investigation of these data is planned for the near future.

5. Summary and discussion

The occurrence of cloud top spots or areas of increased 1.6, 3.7 or 3.9 μm reflectivity and plumes above US storms has been validated. Moreover, the observations have revealed new information on the lifetimes and location of these features with respect to internal storm structure, which was impossible without GOES-8, 9, 10 and NEXRAD data. Though several cases have been documented in which a spot or larger areas of high 3.9 μm reflectivity appeared soon after mesocyclone formation, some other supercell storms on the same day and in the same area had no observable increase in 3.9 μm reflectivity. On the basis of satellite imagery alone, it is difficult to unequivocally link internal storm structure to the occurrence of spots/areas of increased 3.9 μm . However, a much larger sample of cases is needed to determine the significance (if any) of these features with respect to environmental parameters such as freezing level, updraft speed, mixing ratio, shear, etc.

At this time, we do not have any definitive explanations for the origins of spots. However, there might be a possible link between the 3.9 μm spots and “stratospheric” cirrus as observed from aircraft flying at anvil top levels (Fujita, 1982). This cirrus, “jumping up” above anvil tops downwind of overshooting towers as these collapse (Fujita’s proposed explanation of stratospheric cirrus generation), is likely to be composed of smaller particles than was the case for the original distribution within the anvil top (due to gravitational settling). Although Fujita (1982) has reported the “stratospheric” cirrus to extend great distances from its source, one of the authors of this paper (MS) has observed (on 24 May 1996, while flying commercially over Alabama and Georgia) similar “jumping cirrus” to occur on significantly smaller scales (Fig. 6), corresponding to the size range of the 3.9 μm spots. Perhaps, some of the observed 3.9 μm spots (those which remain near overshooting tops during their lifetimes) could alternatively be attributed to pileus clouds.

In contrast to smaller-scale spots or plumes, increased 3.7 or 3.9 μm reflectivity encompassing the entire storm top suggests that the size or geometry of ice crystals throughout the anvil top is different as compared to cloud tops of other storms. The reason for the difference in hydrometeor size is unknown at this time. However, no direct inferences about storm intensity or character, based on the 3.7 or 3.9 μm reflectivity alone, seem to be possible at this time.

A plume typically appears above a Cb anvil in VIS/near IR channels (GOES channel 1, AVHRR channels 1 and 2) rather than in 3.7 or 3.9 μm channels. However, this inconsistency with earlier European observations (Setvák and Doswell, 1991) could result from the timing of the observations. European cases were mostly captured by NOAA 9 or 11 satellites, which were both at later afternoon orbits (at least for part of their lifetime) than the NOAA 14 and 16 observations in the Great Plains. Thus, NOAA 14 depicts storms that are typically at an earlier stage of their development than the other two satellites. The “aging” of the sensors (resulting in a drift of sensor calibration and increase



Fig. 6. Example of “jumping cirrus” above anvil cloud tops. Original slide was taken on 24 May 1996 late afternoon from Delta airliner above Alabama and Georgia. Photo Martin Setvak.

of signal to noise level) may have also impacted these comparisons for some of the NOAA satellites. In contrast, NOAA 12’s early evening orbit lacks sufficient $3.7\ \mu\text{m}$ illumination, and scattering geometry is also much different from mid-afternoon orbits of NOAA 9 and 11. With respect to plumes in GOES-8, 9, 10 imagery, too few data sets have been examined so far to evaluate statistics concerning the plume types.

A mechanism for lifting above anvil level is uncertain at this time. The fact that plumes typically emanate from near the location of warm wakes is surprising given that others have suggested sinking motion in these regions (e.g., Adler and Mack, 1986).

If the plumes were to be explained by some kind of wake effect downstream from an overshooting top or by Fujita’s stratospheric cirrus, a correlation between plume formation/weakening and maximum radar echo height should be expected. Any attempt to find such a link is unlikely, owing to a large ambiguity in echo heights as determined from NEXRAD data. However, the relatively uniform production of plumes as compared to the intermittent nature of overshooting tops makes these explanations uncertain.

Though the mechanism that creates plumes remains unknown, their persistency indicates that they are likely to be found over long-lasting storms, perhaps supercells. This seems to be supported by their frequent simultaneous occurrence with cold-U/warm spot couplets, which are considered to be indicators of possible supercells (McCann, 1983). If this is substantiated, plumes above anvils could be presumed to be another indirect satellite indicator of supercell storms (especially in regions that lack Doppler-radar coverage). We certainly cannot claim that all supercells are accompanied by plumes above anvils, but if a well-defined, distinct plume is observed, the storm may well be a supercell.

However, such a link needs to be validated by a study with a statistically significant number of cases.

In addition, more insight about storm top structures such as plumes or cold-U/warm spot couplets could be developed from high-level flying aircraft observations (multispectral imagery, cloud-top altitude measurements, in-situ measurements of microphysics within plumes, etc.). We regret the absence of any recent airborne observations, such as those collected by Fujita (1982), to complement the WSR-88D and GOES-8, 9 measurements.

Finally, the present studies have shown that the 1.6 and 3.7 or 3.9 μm bands depict similar features (or cloud top morphology). However, the limited number of cases investigated so far precludes any conclusive statements about the advantages of one of these bands versus the other for studies of cloud top microphysics or cloud classification. For cloud studies and monitoring, a combination of both of these bands appears as ideal, which will be achieved with MSG-1 becoming operational by the end of 2003.

Acknowledgements

This research was supported by the US/Czechoslovak Science and Technology Program (Project #94067) and the Grant Agency of the Czech Republic (Grant #205/00/1451). The authors wish to thank Pavel Hampl from CHMI for his software support when processing AVHRR data, Daphne Zaras of NSSL for her processing of radar and GOES satellite data, Julie Adolphson and Patrick Dills of UCAR/COMET, Jim Purdom and John Weaver of NESDIS/RAMM for providing archived and real-time GOES-8 data. One of the authors (VL) wishes to acknowledge funding from EURAINSAT, a shared-cost project (Contract EVG1-2000-00030), co-funded by the Research DG of the European Commission within the RTD Activities of a Generic Nature of the Environment and Sustainable Development sub-programme (5th Framework Programme).

References

- Adler, R.F., Mack, R.A., 1986. Thunderstorm cloud top dynamics as inferred from satellite observations and cloud top parcel model. *J. Atmos. Sci.* 43, 1945–1960.
- Detwiler, A.G., Smith, P.L., Stith, J.L., 1992. Observations of microphysical evolution in a High Plains thunderstorm. *Proc. 11th Int. Conf. on Clouds and Precipitation*, vol. 1. International Commission on Clouds and Precipitation and International Association of Meteorology and Atmospheric Physics, Montreal, PQ, Canada, pp. 260–263.
- Doviak, R.J., Zrnić, D.S., 1984. *Doppler Radar and Weather Observations*. Academic, San Diego, CA.
- Fujita, T.T., 1982. Principle of stereographic height computations and their applications to stratospheric cirrus over severe thunderstorms. *J. Meteorol. Soc. Jpn.* 60, 355–368.
- Goodrum, G., Kidwell, K.B., Winstom, W. (Eds.), 2000. NOAA KLM User's Guide. US Department of Commerce, NOAA/NESDIS, latest version available at: <http://www2.ncdc.noaa.gov/docs/klm/>.
- King, M.D., Kaufman, Y., Menzel, W.P., Tanré, D., 1992. Remote sensing of cloud, aerosol, and water vapor properties from the Moderate Resolution Imaging Spectrometer (MODIS). *IEEE Trans. Geosci. Remote Sens.* 30, 1–27.
- Levizzani, V., Setvák, M., 1996. Multispectral, high-resolution satellite observations of plumes on top of convective storms. *J. Atmos. Sci.* 53, 361–369.

- Maddox, R.A., Zaras, D.S., MacKeen, P.L., Gourley, J.J., Rabin, R.M., Howard, K.W., 1999. Echo height measurements with the WSR-88D: use of data from single versus two radars. *Weather Forecast.* 14, 455–460.
- McCann, D.W., 1983. The enhanced-V, a satellite observable severe storm signature. *Mon. Weather Rev.* 111, 887–894.
- Melani, S., Cattani, E., Levizzani, V., Cervino, M., Torricella, F., 2003. Radiative effects of simulated cirrus clouds on top of a deep convective storm in METEOSAT Second Generation SEVIRI channels. *Meteorol. Atmos. Phys.* 83, 109–122.
- Melani, S., Cattani, E., Torricella, F., Levizzani, V., 2003. Characterization of plumes on top of a deep convective storm using AVHRR imagery and radiative transfer model simulations. *Atmos. Res.* 67–68, 485–499.
- Menzel, W.P., Purdom, J.F.W., 1994. Introducing GOES-I: the first of new generation of Geostationary Operational Environmental Satellites. *Bull. Am. Meteorol. Soc.* 75, 757–781.
- Nakajima, T., King, M.D., 1992. Asymptotic theory for optically thick layers. *Appl. Opt.* 31, 7669–7683.
- Nakajima, T.Y., Nakajima, T., 1995. Wide-area determination of cloud microphysical properties from NOAA AVHRR measurements for FIRE and ASTEX regions. *J. Atmos. Sci.* 52, 4043–4059.
- Rasmussen, E.N., Straka, J.M., Davies-Jones, R., Doswell III, C.A., Carr, F.H., Eilts, M.D., MacGorman, D.R., 1994. Verification of the Origins of Rotation in Tornadoes Experiment (VORTEX). *Bull. Am. Meteorol. Soc.* 75, 995–1006.
- Rosenfeld, D., Cattani, E., Melani, S., Levizzani, V., 2002. Considerations in daylight operation of 1.6 μm vs. 3.7 μm channel on NOAA and Metop satellites. *Proc. Meteorological Satellite Data User's Conf. EUMETSAT, Darmstadt, Germany.*
- Schmetz, J., Pili, P., Tjemkes, S., Just, D., Kerkmann, J., Rota, S., Ratier, A., 2002. An introduction to Meteosat Second Generation (MSG). *Bull. Am. Meteorol. Soc.* 83, 977–992.
- Setvák, M., 1989. Convective storms—the AVHRR channel 3 cloud top reflectivity as a consequence of internal processes. *Proc. 5th WMO Conf. on Weather Modification and Applied Cloud Physics, Beijing, WMO TD-No. 269.* WMO, Geneva, Switzerland, pp. 109–112.
- Setvák, M., Doswell III, C.A., 1991. The AVHRR channel 3 cloud top reflectivity of convective storms. *Mon. Weather Rev.* 119, 841–847.
- Storm Data (NOAA), 1995. National Climatic Data Center/National Oceanic and Atmospheric Administration, ISSN:0039-1972, Vol. 37, No. 12.
- Wang, P.K., 2001. Plumes above thunderstorm anvils and their contributions to cross tropopause transport of water vapor in midlatitudes. *Proc. 11th Conf. Satellite Meteor. Oceanography. AMS,* pp. 161–164.